Eng. Sci., 2025, **38**, 1889

Engineered Science
DOI: https://dx.doi.org/10.30919/es1889

When Traditional Chinese Pigments meet *Stellera chamaejasme L.* on Qinghai-Tibet Plateau: Stability or Fading upon Exposure to Light?

Ting Huang,[1,2,3] Shuliang Li,[1,2,*] Xinlei Hou,[1,2,3] Min Pan,[2,4] Xiaoliang Wang,[1,2] Bing Zhao[1,2] and Xianmin Mai[1,2,*]

Abstract

Traditional architectural paintings, particularly those in the Qinghai-Tibetan Plateau, face significant color fading due to high UV radiation, threatening their artistic and cultural value. This study investigates *Stellera chamaejasme L.*, a native plant, as a natural UV protectant for traditional pigments, including cinnabar, orpiment, realgar, malachite, and azurite. UV-photoaging tests revealed that *Stellera chamaejasme L.* enhances UV absorption, significantly improving pigment stability. UV-vis spectroscopy confirmed its strong photoprotective effect, while XRD and FTIR analyses demonstrated its ability to preserve crystal structures and inhibit carbonyl group decomposition. Chromatic variation (ΔE) measurements showed that pigments treated with *Stellera chamaejasme L.* exhibited 48.1–75.7% less fading compared to untreated samples, with notable efficacy for cinnabar, orpiment, and realgar. Due to its abundance in the Qinghai-Tibetan Plateau, ease of application, and light stability, *Stellera chamaejasme L.* offers a sustainable, eco-friendly solution for conserving traditional architectural paintings. This research provides a promising green approach to mitigating UV-induced degradation in cultural heritage.

Keywords: Qinghai-tibetan plateau; Traditional chinese pigment; *Stellera chamaejasme L.* extract; UV absorber; Anti-photoaging.
Received: 19 June 2025; Revised: 06 November 2025; Accepted: 10 November 2025
Article type: Research article.

1. Introduction

The fading of traditional architectural paintings can affect surface information, artistic expression and cultural heritage. Traditional Chinese pigments applied in Qinghai-Tibetan Plateau are among those particularly prone to color loss due to the complex environment. Among these environmental factors, light is the one that cannot be ignored. The intensity of light radiation in plateau areas is several times higher than that in plains. The intensity of light radiation increases with altitude, especially ultraviolet (UV) radiation. The intensity of UV radiation increases by more than 1.3% for every 100 meters of elevation, and on the plateau at an altitude of 4000 m, the intensity of ultraviolet radiation at a wavelength of 300 nm increased by a factor of 2.5 compared with that on the plains.[1] The solar radiation recorded from typical days in each season across Qinghai-Tibetan Plateau with an average altitude of about 3400 meters, which shows Qinghai-Tibetan Plateau sustains a cumulative solar radiation exceeding 1000 W/m^2 for at least 2.5 hours daily under clear weather conditions (Fig. S1). Unfortunately, the high radiation characteristics of the plateau region, especially in the role of ultraviolet radiation, resulting in a large number of traditional architectural color paintings in Qinghai-Tibetan Plateau appear serious fading phenomenon. Under the accumulated high radiation for a long period of time, this has ultimately led to the varying degrees fading of the pigment layer in many instances in Qinghai-Tibetan Plateau (Fig. S2). Therefore, it is urgent to develop protective materials that protect against ultraviolet light.

The discoloration of traditional pigments in the process of photoaging and its principle have been studied. Scholars have primarily focused on the interaction between the light environment and pigment coloration in polychrome artifacts,[2-4] elucidating how photo-induced oxidation leads to fading, resulting in the loss of color brightness, contrast, and original chromaticity. Concurrently, accelerated photoaging experiments have been employed to investigate the stability patterns of pigments.[5,6] Cinnabar changes from α-HgS hexagonal crystal to β-HgS cubic crystal under long-term light

[1]*School of Architecture, Southwest Minzu University, Chengdu, 610041, China*
[2]*Chengdu Research Base of China-Portugal Joint Laboratory of Cultural Heritage Conservation Science supported by the Belt and Road Initiative, Chengdu, 610041, China*
[3]*School of Economics, Southwest Minzu University, Chengdu, 610041, China*

radiation, the color gradually changes from bright red to dark red;[7-10] Direct light illumination triggers the degradation of arsenic sulfide pigments (realgar and orpiment) and generation of arsenite;[11-16] Azurite and malachite with good UV blocking property are reported to be more stable to photoaging.[17] From the above light photoaging research on traditional Chinese pigments, it can be seen that long-term light exposure especially ultraviolet radiation will lead to the damage of internal structure of pigments and discoloration. Therefore, it is urgent to improve the anti-photoaging performance of traditional Chinese pigments, especially when the application scenarios of these pigments are high plateaus.

In addition to technical approaches involving appropriate light source regulation,[18-20] traditional pigment conservation method is to use polymers as surface sealants, adhesives and reinforcing agents, such as epoxy and acrylic acid. But these polymers are prone to photo-oxidation.[21,22] For example, epoxy-treated artifacts can turn yellow under prolonged UV exposure, affecting the original appearance of the paint;[23] Acrylic resin is ultraviolet-transparent. Photoaging will cause chain-breaking and cross-linking reactions of acrylic resins and thus reduce bonding performance, cause chalking,[24] and even toxicity.[25,26] Additionally, nano materials are used in the field of conservation and restoration of traditional pigments.[27-32] For example, titanium dioxide with photocatalytic activity is used to improve the UV resistance of traditional pigments;[33-35] Nano SiO_2 has a strong ultraviolet reflection with an ultraviolet reflectance of more than 70%.[36,37] Nano SiO_2 modified Paraloid B72 exhibited good surface protection performance for colored paintings with properties of UV resistance and small appearance change to samples. Although nanomaterials have good UV resistance, they have the disadvantages of photoinduced discoloration, potential environmental pollution, harm to human bodies, and agglomeration.[38] Therefore, simple and low-cost preparation, eco-friendly, UV resistant and high-performance protective materials are urgently needed.

A growing body of research in recent years has validated the potential of various plant resources for enhancing material photostability.[39-43] These studies have elucidated the mechanisms of natural photoprotective agents, with a particular focus on their ultraviolet absorption and antioxidant properties. For example, flavonoids which are found in the roots, stems, leaves, flowers and fruits of higher plants have strong ultraviolet absorption property. Sunscreen with flavonoids extracted from aloe vera and Baicalin shows SPF value of up to 30 or more;[44-46] Anthraquinones,[47] lignans[48] and polysaccharides[49,50] are widely found in plants and have been confirmed to perform antioxidant and anti-UV effects, the mechanism of which may be related to the enhancement of anti-oxidizing component activity and reduction of oxygen radicals. In studies on the composition of the natural plant *Stellera chamaejasme L.*, it has been found to contain compounds such as tannins, lignin, flavonoids, volatile oils, phenols, terpenoids and other compound components.[51-57] Existing research has confirmed that these compounds possess the potential to be applied as UV-shielding additives. Although natural plant extracts still face limitations in terms of UV protection stability, bioavailability, and broad-spectrum performance, their environmentally friendly nature and multifunctional advantages provide a theoretical foundation for this study's exploration of the protective effects of *Stellera chamaejasme L.* extract on mineral pigments.

In conclusion, research on the lightfastness of traditional pigments has garnered significant attention in the field of cultural heritage conservation. Current protective approaches primarily involve modulating the light environment or applying nanoscale coatings, which methods often characterized by complex preparation processes and potential environmental and health risks. While recent studies have confirmed the efficacy of natural plant extracts in resisting photoaging, their application to the protection of architectural heritage materials remains underexplored. *Stellera chamaejasme L.* has grown widely in Qinghai-Tibetan Plateau and is used as raw material for Tibetan paper. Leveraging its local availability, eco-friendly and simple extraction process, and compatibility with traditional techniques, this study explores its potential as a sustainable and particularly suitable alternative for the conservation and restoration of architectural heritage in high-altitude regions. Therefore, this study aims to simulate the plateau light environment and explore the effect of *Stellera chamaejasme L.* on the fading performance of traditional Chinese pigments. The suitability and effectiveness of the *Stellera chamaejasme L.* extract was demonstrated and the intrinsic mechanism of anti-photoaging of the modified pigments was analyzed through a multi-analytical approach including surface and chemical-physical analyses. To provide the plateau plant *Stellera chamaejasme L.* as an anti-photoaging material for the ecological conservation of paintings pigments, promoting sustainability in architectural heritage preservation practices.

2. Materials and methods

2.1 Materials and specimen preparation

2.1.1 Pigments

The pigments come from artisans of Qinghai-Tibetan Plateau, and were identified as cinnabar, orpiment, realgar, malachite, and azurite through XRD (X-ray diffraction) (Fig. 1).

2.1.2 Preparation of *Stellera chamaejasme L.* extract

The primary extraction process of *Stellera chamaejasme L.* root involves several key steps: First, the root is crushed and then soaked in ethanol at a ratio of 1:10-30 for 5-10 days. During this period, the volume of ethanol is reduced to one-

[4]*School of Chemistry and Environment, Southwest Minzu University, Chengdu, 610041, China*

**Email:* lishuliang@swun.edu.cn (Shuliang Li), maixianmin@foxmail.com (Xianmin Mai)

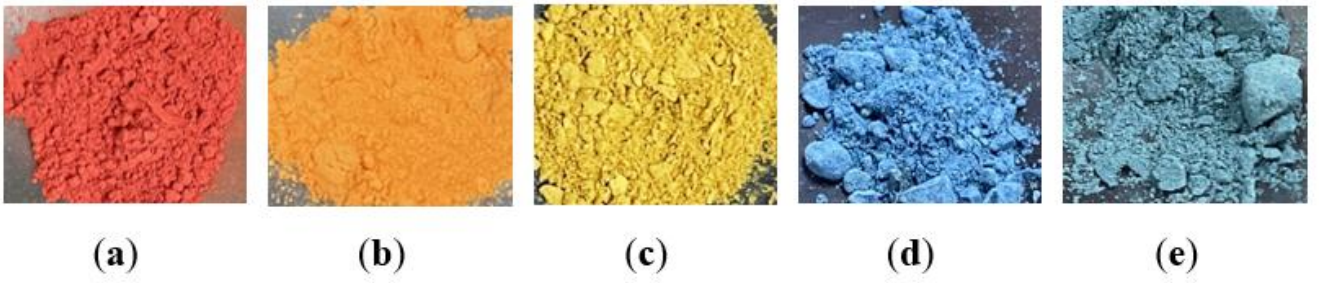

Fig. 1: Pigments: (a) Cinnabar;(b) Orpiment;(c) Realgar;(d) Azurite; (e) Malachite.

Fig. 2: *Stellera chamaejasme L.* extract process flow diagram.

tenth through evaporation. Following this, the mixture is cooled and subjected to desugarization for 2-4 days before further concentration to yield a paste of the primary extract from *Stellera chamaejasme L.* Subsequently, for application purposes, this primary extract paste is combined with ethanol in a weight ratio of 1:20-25 and thoroughly dissolved using ultrasonic stirring to produce the final *Stellera chamaejasme L.* extract. Fig. 2 illustrates the flow diagram of the extraction process.

2.1.3 Preparation of *Stellera chamaejasme L.* modified pigments

Five different colors of traditional Chinese pigments were mixed with *Stellera chamaejasme L.* extract in the following weight ratios: 3:1, 5:1, 1:1, 1:3, and 1:5. The mixtures of *Stellera chamaejasme L.* extract and traditional pigments were placed into new Petri dishes sequentially and stirred thoroughly to ensure homogeneity. Then, they were allowed to stand for 24 hours to dry completely, the modified pigments were ground into fine powder with a mortar and pestle, followed by sieving to achieve consistent particle size distribution for subsequent testing accuracy.

2.2 Lighting conditions and accelerated fading chamber

The light source utilized is the CEL-HXF300-T3 xenon lamp manufactured by Beijing Zhongjiao Jinyuan Science and Technology Co., Ltd. The spectral range of the xenon light source range from 300 nm to 2500 nm and UV output of 2.6W. This xenon lamp system provides stable illumination over extended periods, as illustrated in Fig. S3, which depicts the platform for simulating a plateau light environment. The solar power pyranometer (TES-1333R, TES Electrical Electronic Corp.) is employed for monitoring the simulated light environment, maintaining light radiation intensity between 1000-1100 W/m². Concurrently, with temperature maintains about 48°C and relative humidity maintained at around 46%. Surface temperatures of red and yellow pigments were approximately 50°C, while those of blue and green pigments reached about 65°C. The pigments underwent accelerated photoaging under plateau conditions for a duration of 72 hours.

2.3 Color analysis

A high-precision colorimeter, SR-60 by 3nh, is employed to assess the changes in L*a*b* values of various pigments during aging, following CIE standards. The CIE standard colorimetric system facilitates the measurement and calculation of color differences; the three parameters—L*, a*, and b*—can be individually determined: L* indicates brightness, a* represents the balance between red and green, while b* denotes yellow versus blue. For each pigment sample tested, three measurement points were established. In accordance with GB/T 11186.2 and GB/T 11186.3 standards ((GB/T: Guobiao Standard, Chinese National Standard)),[58,59] three sets of Lab values were obtained for each pigment at different time intervals during the photoaging process, from which the mean values and standard deviations were calculated. The color difference between samples and SD values are calculated using the Eq. (1) and Eq. (2). Concurrently, the analysis incorporated the chromatic change grading criteria from GB/T 1766-2008 standard (Table S1).[60]

$$\triangle E* = \sqrt{(\triangle L*)^2 + (\triangle a*)^2 + (\triangle b*)^2} \quad (1)$$

$$SD = \sqrt{\frac{\sum_{i=1}^{n}(x_i - \bar{x})^2}{n-1}} \quad (2)$$

where △E* signifies the overall color difference value, with △L* representing brightness variation, △a* indicating shifts in red-green balance, and △b* reflecting variations in yellow-blue hue. SD represents the sample standard deviation, where x_i denotes the data point of ΔE*, ΔL*, Δa*, or Δb* at the *i*-th time point, $\bar{x}$ is the arithmetic mean of ΔE*, ΔL*, Δa*, or Δb*, n is the total number of samples, and *i* refers to the *i*-th time point.

2.4 Ultraviolet and visible (UV–vis) spectrophotometry

The ultraviolet-visible absorption spectra of *Stellera chamaejasme L.* extract were acquired using a V-1800 UV-Vis spectrophotometer (Shanghai Mapada Instrument Co., Ltd.) with the following specifications: wavelength range of 190–800 nm, spectral bandwidth of 2 nm, wavelength accuracy of ±0.3 nm, and wavelength repeatability of ≤0.2 nm; Reflectance spectra were obtained using a SEK-EX UV-Vis spectrometer (Shanghai Chenchang Instrument Equipment Co., Ltd.) under the conditions: Testing range of 200–550 nm, slit width of 50 μm, resolution of 2.8 nm, incident angle range of 0°–180°, and input power of 9W. Based on the principle of energy conservation, in opaque materials (where no light transmission occurs, i.e., transmittance T=0), the energy of incident light is entirely allocated to reflection and absorption. The collected data were analyzed to calculate the UV absorption rate of the samples, and the Eqs. (3) and (4) are as follows:

$$R_{UV}(\%) = \frac{\int_{0.28}^{0.4} I_{solar}(\lambda) \cdot R(\lambda) d\lambda}{\int_{0.28}^{0,4} I_{solar}(\lambda) d\lambda} \quad (3)$$

$$UV\ absorption\ (\%) = 100 - R_{UV} \quad (4)$$

here, I_{solar} is the ASTM G173 Global solar intensity spectrum ($W.m^{-2}.\ \mu m^{-1}$), λ is the wavelength(μm), *R(λ)* represents any reflectance value (%), R_{UV} is ultraviolet reflectance (%), *UV absorption* is ultraviolet absorption (%).

2.5 Chemical analysis

X-ray diffraction (XRD) analyses under Cu Kα radiation were conducted using a Rigaku Ultima IV from Japan; and Fourier Transform Infrared Spectroscopy (FT-IR) data were obtained using a Thermo Fisher FT-IR200 from America. All spectra were recorded in the wavenumber range of 4000 cm^{-1} to 500 cm^{-1} with a resolution of 4 cm^{-1}.

3. Results and discussion

3.1 Ratio optimization results

As shown in Fig. 3, the extract of *Stellera chamaejasme L.* root has a strong UV-absorption capacity in the range of 200-400 nm, and within its range near 225nm and 290nm have obvious absorption peaks. It demonstrates that *Stellera chamaejasme L.* extract can provide long-term and stable UV protection for materials when exposed to sunlight.

In this study, traditional Chinese pigments are mixed with *Stellera chamaejasme L.* extract in different weight ratios of 1:5, 1:3, 1:1, 3:1 and 5:1; and the modified pigments are dried naturally for 24 hours to form powders, the modified pigment was spread evenly on wooden blocks (0.5cm*0.5cm *0.5cm). After thickness measurement, the thickness of the spread pigment was approximately 0.5 mm.

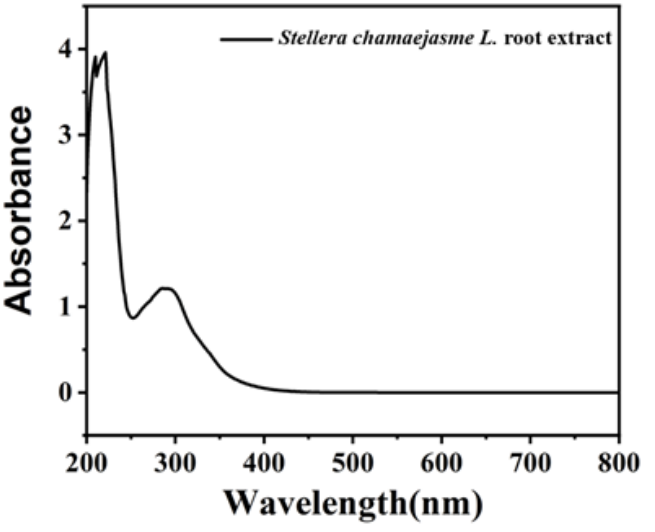

Fig. 3: UV-VIS absorption spectrum of *Stellera chamaejasme L.* root extract.

Under the influence of *Stellera chamaejasme L.*, the UV absorption rate of the modified pigments obviously increased, demonstrating that the plant exhibits UV-absorbing properties. This effectively reduces UV-induced damage to the pigment, such as photodegradation and aging. This improvement endows pigments with enhanced ultraviolet-resistance properties, enabling it to more effectively shield against ultraviolet radiation. Fig. 4 illustrates the UV-vis reflectance of all original and modified pigments. It is evident that the original cinnabar, realgar, and orpiment pigments exhibit relatively low absorption rates for ultraviolet light (Figs. 4a-c), suggesting poor light resistance. In contrast, the original azurite and malachite pigments show absorption rates of up to 90% for ultraviolet light (Figs. 4d, 4e and S4) and absorb energy at specific wavelengths of ultraviolet light in the 200–400 nm wavelength range, thereby reducing the direct damage of UV light to the pigments matrix, indicating their superior ability to resist light exposure. Furthermore, as the concentration of *Stellera chamaejasme L.* extract increases in the modified pigments, their UV-absorption performance can be enhanced to over 85%, particularly for cinnabar, realgar, and orpiment. However, considering that the actual dosage of *Stellera chamaejasme L.* extract is relatively low—potentially diminishing its infiltration effectiveness into the pigment or excessive amounts may adversely affect color chromaticity and the pigment particle size; Therefore, the weight ratio of 1:1 was selected as the optimal parameter for subsequent optimization, ensuring effective extraction efficiency while maintaining chromatic stability (Table S2).

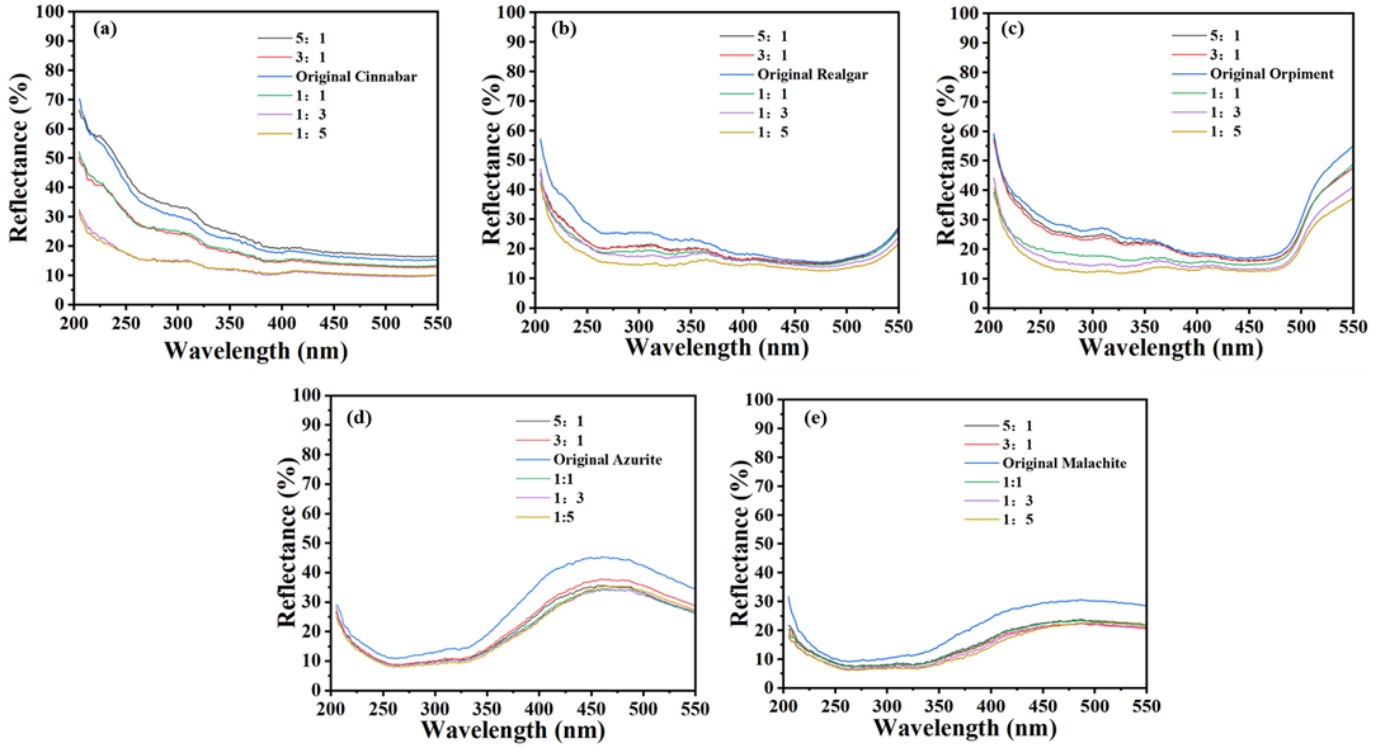

Fig. 4: The UV-vis reflectance of the original pigments and five different pigment formulations containing *Stellera chamaejasme L.* extract:(a) Cinnabar;(b) Realgar; (c) Orpiment, (d)Azurite;(e) Malachite.

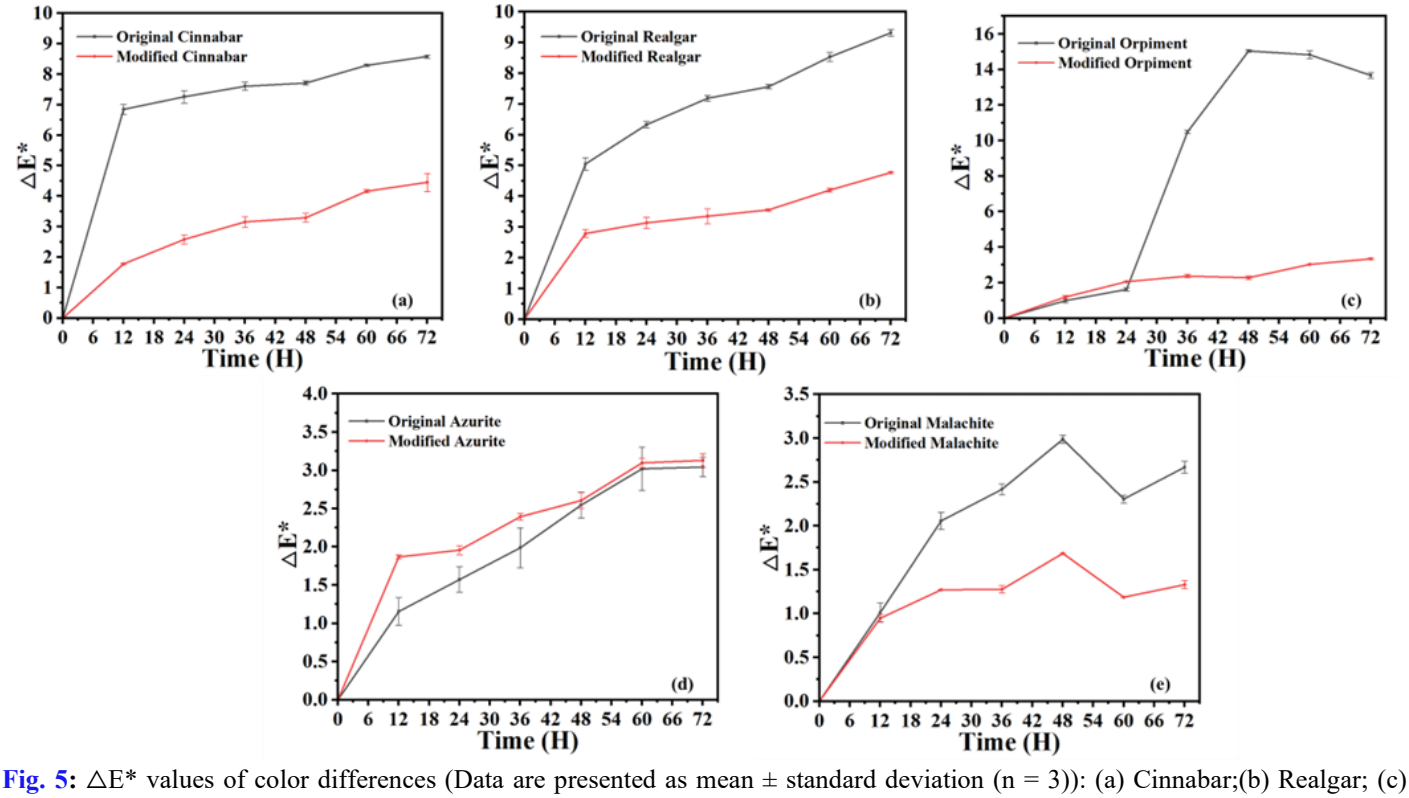

Fig. 5: △E* values of color differences (Data are presented as mean ± standard deviation (n = 3)): (a) Cinnabar;(b) Realgar; (c) Orpiment, (d)Azurite;(e) Malachite.

3.2 Photoaging test results analysis

3.2.1 Light-induced color difference analysis

The △E* values of color differences and the aging changes presented in Fig. 5 and Table S3, provide insights into the degrees of fading for both original and modified pigments. Notably, the original cinnabar, realgar, and orpiment pigments exhibited discoloration obviously; Specifically, the negative △L*, △a*, and △b* values for cinnabar indicate a transition

from bright red to dark red, while changes in realgar and orpiment were primarily reflected in their △a* and △b* values, realgar loses its original red-orange hue to yellow and orpiment turns yellow to white. When *Stellera chamaejasme L.* extract was added to cinnabar and realgar during photoaging (Figs. 5a, 5b), the resulting color difference change was markedly smaller than that of the original pigments, demonstrating an improved color-fixing effect—reducing color difference by factors of 2 respectively compared to their originals. For orpiment pigment treated with *Stellera chamaejasme L.* extract (Fig. 5c), the color difference (△E*) decreased by a factor of 4; Conversely, azurite and malachite pigments underwent photoaging (Figs. 5d, 5e) where their color differences remained below 3.5—indicating minimal change—and only slight reductions were observed after adding *Stellera chamaejasme L.* extract to these pigments' formulations. Furthermore, comparison of pigment chromaticity before and after photoaging illustrated intuitively in Fig. 6 and Fig. S5 show that those containing *Stellera chamaejasme L.* extract faded less than their unmodified counterparts overall; Thus, confirming that incorporating this extract effectively stabilizes traditional pigment colors, especially for cinnabar, realgar and orpiment.

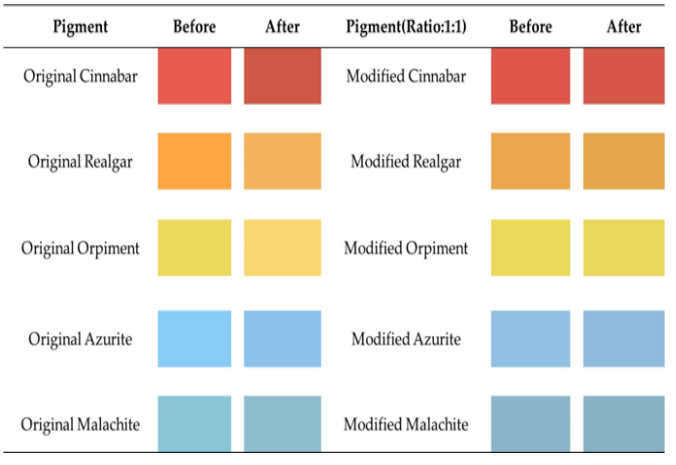

Fig. 6: Comparison of pigment chromaticity before and after photoaging.

3.2.2 Composition and internal structure analysis

X-ray diffraction was employed to analyze the composition of traditional Chinese pigments, matching with the XRD standard card, revealing that the red cinnabar pigment consists of HgS; the orange realgar pigment is composed of As_4S_4; the yellow orpiment pigment contains As_2S_3; the green malachite pigment comprises $CuCO_3(OH)_2$; and the blue azurite pigment consists of $Cu_3(CO_3)_2(OH)_2$.

XRD was further applied to analyze the photoaging results of *Stellera chamaejasme L.* extract modified pigments concerning composition and internal structure. According to the XRD patterns of the original pigments and the modified pigments before photoaging (Fig. 7), there is no obvious disappearance or displacement of the diffraction peaks after adding the extract of *Stellera chamaejasme L.* to the pigments. This indicates that the extract of *Stellera chamaejasme L.* does not cause any changes in the internal structure of the original pigments, and the X-ray absorption effect of the organic components in the *extract of Stellera chamaejasme L.*, the diffraction signal of the modified pigment slight decays.

The XRD analysis the changes of cinnabar before and after photoaging (Figs. 7a,7b), the characteristic diffraction peaks of the original cinnabar pigment before photoaging and the modified cinnabar pigment before and after photoaging correspond to the hexagonal crystal structure of α-HgS. The original cinnabar pigment after photoaging matches well with the standard spectrum of β-HgS, the characteristic diffraction peaks at 2θ=28.17°, 43.59°, 47.8°, and 52.78° exhibit significantly attenuated intensity, with partial peaks evolving toward disappearance. This change indicates that long-term light exposure induces a transformation in the crystal structure. Further analysis reveals that this phase transition involves lattice reconstruction from a hexagonal to a cubic crystal system and phase conversion from α-HgS to β-HgS, directly leading to changes in the material's optical properties, and also explains the observed color change from bright red to dark reddish-brown; The intensity of XRD diffraction peaks for realgar diminishes and narrows under light aging effects (Figs. 7c, 7d). It can be inferred that realgar is chemically unstable and undergoes complex chemical reactions when exposed to light, transforming into pararealgar while simultaneously being reduced to powder form. Pararealgar continues reacting under light conditions until it gradually converts into orpiment and arsenic trioxide (As2O3). Also, the long-term light exposure adversely affects orpiment's XRD peak intensities—resulting in weaker signals that may even disappear entirely over time (Figs. 7e, 7f). In addition, incorporating *Stellera chamaejasme L.* extract into cinnabar, realgar and orpiment pigments yields negligible changes in their respective XRD profiles; Furthermore, observations from Figs. 7g-j reveal that the original azurite and malachite pigments exhibit minimal significant changes before versus after photoaging, indicating their inherent photoaging resistance and the weak protective effect of *Stellera chamaejasme L.* extract on them. Thus, affirming the extract plays a protective role against structural deterioration caused by light exposure for cinnabar, realgar, and orpiment.

Under the same testing environment, FTIR was further applied to analyze the photoaging results of *Stellera chamaejasme L.* extract modified azurite and malachite concerning composition. It can be inferred from Fig. 8 that after the pigment undergoes aging, there are no significant displacement or disappearance of its characteristic peaks. The main change is reflected in the alteration of the infrared absorption intensity. Additionally, the infrared intensity of the modified pigment after photoaging is essentially at the same level as that of the original pigment post-aging. As shown in Fig. 8b, following the addition of *Stellera chamaejasme L. extract*, there is an increase in the overall characteristic peak

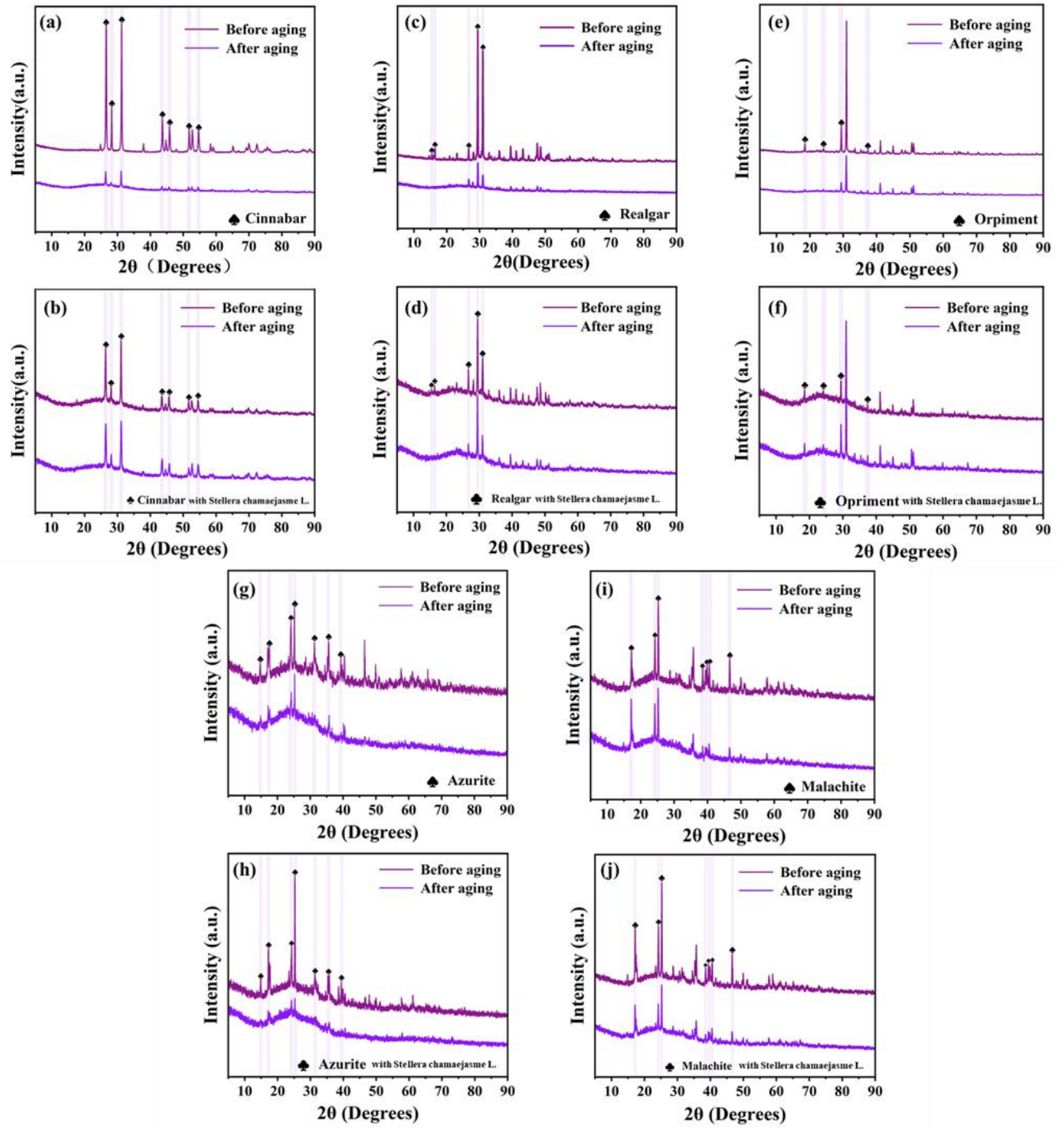

Fig. 7: The XRD of traditional pigments and modified pigments before and after photoaging:(a) Cinnabar: XRD corresponds to α-HgS (ICDD 10897103) and β-HgS (ICDD 60261) ;(b) Cinnabar with *Stellera chamaejasme L.* extract;(c) Realgar: XRD corresponds to As_4S_4 (PDF#51-0782);(d) Realgar with *Stellera chamaejasme L.* extract;(e) Orpiment: XRD corresponds to As_2S_3 (PDF#19-0084);(f) Orpiment with *Stellera chamaejasme L.* extract; (g)Azurite: XRD corresponds to $Cu_3(OH)_2[CO_3]_2$ (PDF#99-0015);(h) Azurite with *Stellera chamaejasme L.* extract; (i) Malachite: XRD corresponds to $Cu_2(OH)_2CO_3$ (PDF#72-0075); (j) Malachite with *Stellera chamaejasme L.* extract.

intensities for azurite. The *Stellera chamaejasme L.* extract is adsorbed on the surface of azurite and gradually penetrates into the interior of the crystal. The hydrogen atoms in the *Stellera chamaejasme L.* extract form hydrogen bonds with the oxygen atoms in the hydroxyl groups or carbonate groups of azurite molecules. This promotes the formation of more hydrogen bonds between the hydroxyl groups (3200-3550cm^{-1}) and carbonate groups (1400-1470 cm^{-1}, 800- 1000 cm^{-1}) within azurite molecules, leading to an increase in the overall infrared absorption intensity of azurite. Moreover, after 72 hours of photoaging, carbonate ions (CO_3^{2-}) gradually decompose into carbon dioxide and oxygen. As the amount of

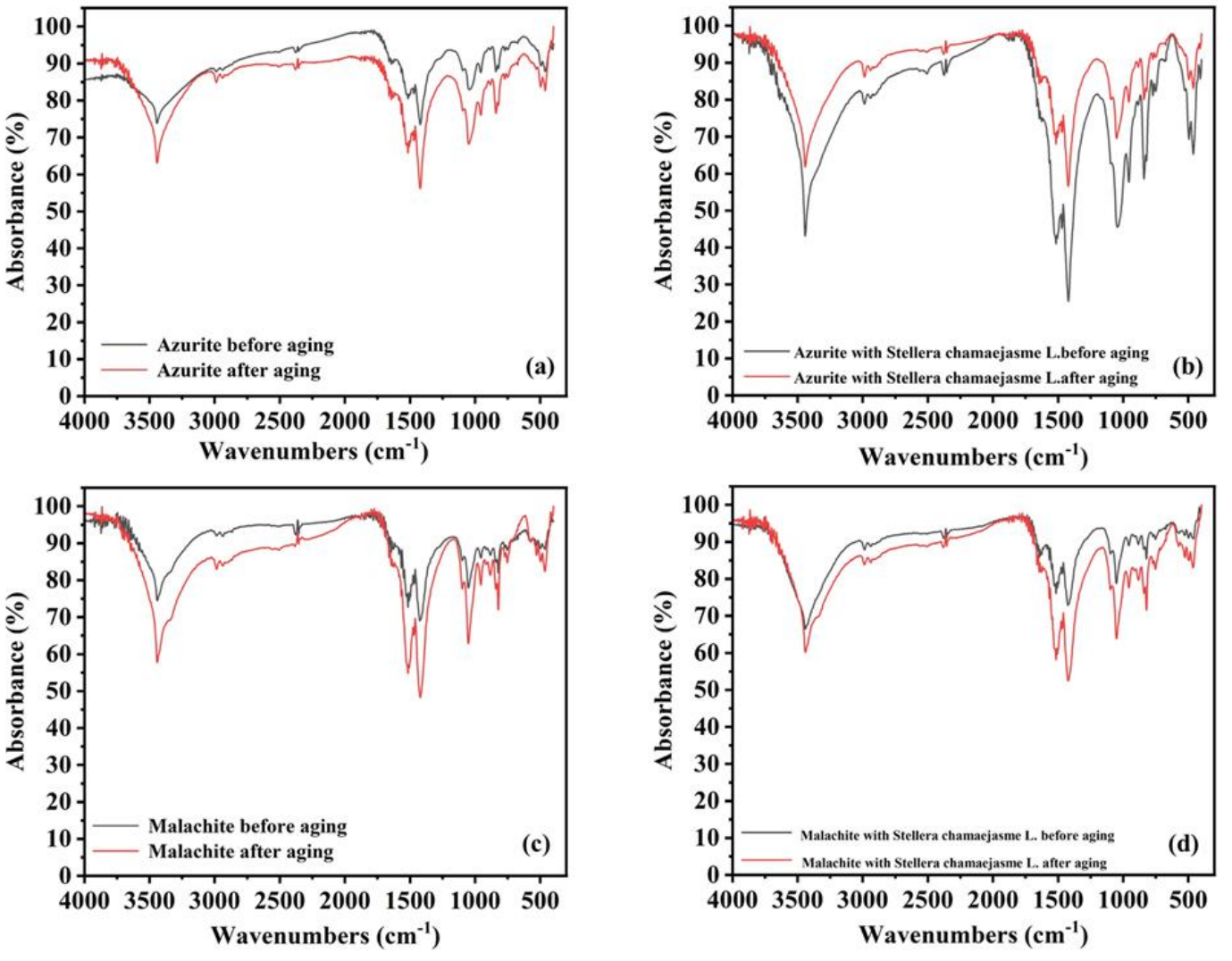

Fig. 8: (a) Infrared spectra before and after aging of original azurite pigment;(b) Infrared spectra before and after aging of azurite pigment with *Stellera chamaejasme L.*; (c) Infrared spectra before and after aging of original malachite pigment;(d) Infrared spectra before and after aging of malachite with *Stellera chamaejasme L.*

carbonate decreases, the corresponding infrared absorption intensity naturally declines. And its infrared intensity remains consistent with that shown in Fig. 8a after aging. This indicates that incorporating *Stellera chamaejasme L.* into azurite pigment does not yield significant effects, which aligns with findings from color analysis. In Fig. 8c and 8d, the sole alteration observed between malachite with *Stellera chamaejasme L.* and its original counterpart pertains to changes in the absorption intensity of hydroxyl O-H characteristic peaks within the range of 3000–3600 cm^{-1}. Notably, alterations in absorption intensity for these hydroxyl O-H peaks are more pronounced in untreated malachite compared to those treated with *Stellera chamaejasme L.*, suggesting that while malachite pigment undergoes changes during light aging, adding this extract mitigates internal transformations within malachite pigments—thereby serving a role as a color fixative, which is consistent with the chromatic aberration analysis and has a certain inhibitory effect.

3.2.3 Durability analysis

The changes in UV absorption capacity of the original pigments before and after photoaging were more pronounced than those with the addition of *Stellera chamaejasme L.* extract, which mainly focuses on the UV absorption rates in the UVA (Δλ= 320-400nm) and UVB (Δλ=280-320nm) bands. As shown in Table 1, the UV absorption rate of the original cinnabar pigment in both the UVA and UVB bands increased by approximately 2% after photoaging (Fig. 9a). This phenomenon is attributed to sulfur oxidation during the phase transition under continuous light exposure, which induces densification of the pigment matrix, reduces photocatalytic active sites of surface sulfides, and reconstructs the crystal lattice to form a more compact Hg-S coordination structure. For the modified cinnabar pigment, the UV absorption rates increased by 5.87% (UVA) and 8.68% (UVB), respectively, and remained stable after photoaging with minimal variation. In Figs. 9b and 9c, the UV absorption rates of realgar and orpiment pigments decreased by approximately

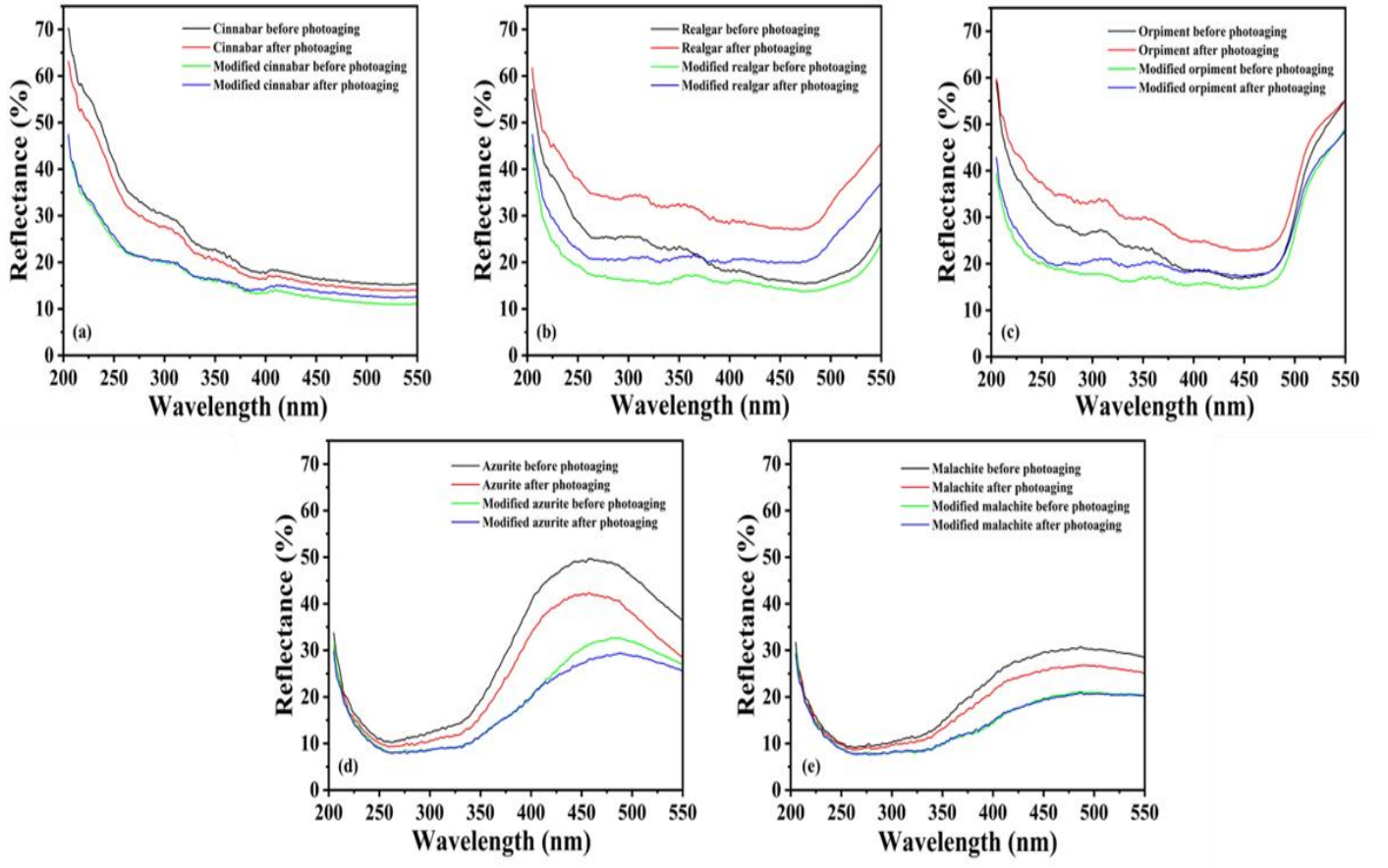

Fig. 9: UV–vis reflectance spectra of the original pigments and the modified pigments before and after photoaging: (a) Cinnabar; (b) Realgar; (c) Orpiment; (d) Azurite;(e) Malachite.

Table 1: UV absorption rates of traditional Chinese pigments and modified pigments before and after photoaging.

Pigment	Photoaging	UVA absorption (%)	UVB absorption (%)	Modified pigment	Photoaging	UVA absorption (%)	UVB absorption (%)
Cinnabar	Before	78.95	70.39	Cinnabar	Before	84.82	79.07
	After	80.71	72.94		After	84.44	80.28
Realgar	Before	78.18	75.04	Realgar	Before	83.93	84.00
	After	69.21	66.43		After	79.56	79.45
Orpiment	Before	78.30	73.66	Orpiment	Before	83.78	82.46
	After	71.89	67.1		After	80.72	79.77
Azurite	Before	75.93	87.77	Azurite	Before	86.64	91.42
	After	80.13	89.50		After	86.6	91.47
Malachite	Before	80.16	89.77	Malachite	Before	87.48	92.02
	After	82.48	90.55		After	87.24	92.00

9% and 6.5% respectively after photoaging. In contrast, the modified realgar exhibited increased UV absorption rates of 5.75% (UVA) and 9% (UVB), while the modified orpiment showed increases of 5.48% (UVA) and 8.8% (UVB). Although the UV absorption rates of the modified pigments decreased after photoaging, they were still consistently higher than those of their respective original pigments before photoaging. Conversely, Figs. 9d and 9e demonstrate that the original

azurite and malachite pigments inherently exhibit strong UV absorption peaks in the 200–400 nm range, with slight increases in UV absorption post-aging. The variations in UV absorption capacity between original and modified azurite and malachite before and after photoaging were negligible, indicating that the *Stellera chamaejasme L.* extract exhibits a relatively weak protective effect on them. Notably, after the addition of *Stellera chamaejasme L.* extract, the UV absorption rates of cinnabar, realgar, and orpiment remain relatively stable after photoaging, are better than those of the original pigments before photoaging, and exhibit smaller changes before and after photoaging. Furthermore, the magnitude of UV absorption rate changes before and after photoaging was significantly reduced, indicating that the UV-absorbing properties of the extract effectively shield the pigments by absorbing ultraviolet radiation, thereby retarding their photoaging degradation.

4. Conclusion

In conclusion, this study systematically confirms the distinct photodegradation behaviors of traditional mineral pigments: while cinnabar (HgS), realgar (As_4S_4), and orpiment (As_2S_3) exhibit pronounced photosensitivity and severe fading upon photoaging, azurite $Cu_3(CO_3)_2(OH)_2$ and malachite $CuCO_3(OH)_2$ demonstrate superior lightfastness and chromatic stability. Furthermore, we have demonstrated a simple, eco-friendly, and cost-effective method for enhancing pigments UV radiation resistance by combining *Stellera chamaejasme L.* extract with traditional Chinese pigments. This novel color-fixing material demonstrates particularly applicability for architectural polychromy preservation in Qinghai-Tibet Plateau. The *Stellera chamaejasme L.* extract exhibits UV-absorbing capabilities, significantly improving the UV absorption efficiency of modified pigments, particularly for light-sensitive cinnabar, realgar, and orpiment pigments. Moreover, this phytochemical intervention not only preserves the original chromatic characteristics but also safeguards the structural integrity of pigment matrices against photochemical degradation. This study paves an innovative way for developing protective coatings tailored to plateau architectural heritage, bridging traditional craftsmanship with sustainable conservation science, and providing an environmentally preservation strategy for plateau cultural relics, thereby ensuring the sustainable restoration of these vulnerable heritage sites.

Acknowledgments

The authors are very grateful for financial support from National Key R&D Program of China (2024YFC3808304), MOE (Ministry of Education in China) Liberal arts and Social Sciences Foundation, National Natural Science Foundation of China (22376173), Natural Science Foundation of Sichuan Province (2024NSFSC0994), Chengdu Science and Technology Project (2024-YF05-00889-SN), and the Project of Qinghai-Tibetan Plateau Research in Southwest Minzu University (2024CXTD06) and the 2025 Graduate Students' Innovative Research project in Southwest Minzu University

Institutional Review Board Statement

Not applicable.

Informed Consent Statement

Not applicable.

Data Availability Statement

The original contributions presented in the study are included in the article, further inquiries can be directed to the corresponding author

Conflict of Interest

The authors declare no conflict of interest.

Supporting Information

Applicable.

CRediT Statement

Ting Huang and **Shuliang Li:** Conceptualization. **Ting Huang**, **Min Pan** and **Xinlei Hou:** Investigation. **Ting Huang:** Resources. **Ting Huang** and **Shuliang Li:** Data curation. **Ting Huang:** Writing - Original draft preparation. **Shuliang Li:** Writing - Review and Editing. **Xiaoliang Wang:** Visualization. **Bing Zhao** and **Xianmin Mai:** Supervision. **Bing Zhao** and **Xianmin Mai:** Project administration. All authors have read and agreed to the published version of the manuscript.

References

[1] M. Blumthaler, W. Ambach, R. Ellinger, Increase in solar UV radiation with altitude, *Journal of Photochemistry and Photobiology B*: *Biology*, 1997, **39**, 130-134, doi: 10.1016/s1011-1344(96)00018-8.

[2] H. Y. Chun, S. Y. Lee, J. I. Sohn, Degradation mechanisms of traditional pigments used in historic artworks within national heritage temple halls, *Korean Journal of Chemical Engineering*, 2025, **42**, 3269-3276, doi: 10.1007/s11814-025-00518-w.

[3] E. Avranovich Clerici, S. de Meyer, F. Vanmeert, S. Legrand, L. Monico, C. Miliani, K. Janssens, Multi-scale X-ray imaging of the pigment discoloration processes triggered by chlorine compounds in the upper basilica of saint francis of Assisi, *Molecules*, 2023, **28**, 6106, doi: 10.3390/molecules28166106.

[4] I. G. da Silva, I. de Souza Reis, R. W. de Assis Franco, B. Sanchez, M. C. Canela, Effect of volatile organic compounds on the stability of inorganic pigments in oil-based paintings, *Journal of Cultural Heritage*, 2025, **73**, 277-285, doi: 10.1016/j.culher.2025.03.011.

[5] T. Vitorino, M. Picollo, J. M. del Hoyo-Mel é ndez, An investigation of the photostability of 19th century artists ' cochineal lake pigments using MFT and conventional accelerated

ageing tests, *Nondestructive Testing and Evaluation*, 2024, **39**, 2530-2548, doi: 10.1080/10589759.2024.2304261.
[6] F. K. Al-Kadi, J. F. Abdulkareem, B. A. Azhdar, Hybrid chitosan – TiO_2 nanocomposite impregnated in type A-2186 maxillofacial silicone subjected to different accelerated aging conditions: an evaluation of color stability, *Nanomaterials*, 2023, **13**, 2379, doi: 10.3390/nano13162379.
[7] M. K. Neiman, M. Balonis, I. Kakoulli, Cinnabar alteration in archaeological wall paintings: an experimental and theoretical approach, *Applied Physics A*, 2015, **121**, 915-938, doi: 10.1007/s00339-015-9456-x.
[8] I. Galain, P. B. María, A. Ivana, F. Laura, Hydrothermal synthesis of alpha- and beta-HgS nanostructures, *Journal of Crystal Growth*, 2017, **457**, 227-233, doi: 10.1016/j.jcrysgro.2016.08.066.
[9] J. Yang, W.-H. Zhang, Y.-P. Hu, J.-S. Yu, Aqueous synthesis and characterization of glutathione-stabilized β -HgS nanocrystals with near-infrared photoluminescence, *Journal of Colloid and Interface Science*, 2012, **379**, 8-13, doi: 10.1016/j.jcis.2012.04.057.
[10] J. K. McCormack, The darkening of cinnabar in sunlight, *Mineralium Deposita*, 2000, **35**, 796-798, doi: 10.1007/s001260050281.
[11] J. Harrison, J. Lee, B. Ormsby, D. J. Payne, The influence of light and relative humidity on the formation of epsomite in cadmium yellow and French ultramarine modern oil paints, *Heritage Science*, 2021, **9**, 107, doi: 10.1186/s40494-021-00569-2.
[12] F. T. H. Broers, K. Janssens, J. Nelson Weker, S. M. Webb, A. Mehta, F. Meirer, K. Keune, Two pathways for the degradation of orpiment pigment (As_2S_3) found in paintings, *Journal of the American Chemical Society*, 2023, **145**, 8847-8859, doi: 10.1021/jacs.2c12271.
[13] A. Macchia, L. Campanella, D. Gazzoli, E. Gravagna, A. Maras, S. Nunziante, M. Rocchia, G. Roscioli, Realgar and light, *Procedia Chemistry*, 2013, **8**, 185-193, doi: 10.1016/j.proche.2013.03.024.
[14] X. Zhang, Progress in the Study of Light Induced Alteration of Realgar, *Acta Geoscientica Sinica*, 2017, **38**, 223-228, doi:10.3975/cagsb.2017.02.14.
[15] J. Simoen, S. De Meyer, F. Vanmeert, N. de Keyser, E. Avranovich, G. Van der Snickt, A. Van Loon, K. Keune, K. Janssens, Combined Micro- and Macro scale X-ray powder diffraction mapping of degraded Orpiment paint in a 17th century still life painting by Martinus Nellius, *Heritage Science*, 2019, **7**, 83, doi: 10.1186/s40494-019-0324-4.
[16] D. J. E. Mullen, W. Nowacki, Refinement of the crystal structures of realgar, AsS and orpiment, As_2S_3, *Zeitschrift Für Kristallographie*, 1972, **136**, 48-65, doi: 10.1524/zkri.1972.136.1-2.48.
[17] X. Zhou, X. Li, Study on the stability of stone green mineral pigment in ancient paintings, *Applied Chemical Engineering*, 2016, **45**, 245-248, doi: 10.16581/j.cnki.issn1671-3206.20151224.050.
[18] K. Ghosh, A. Mondal, Some studies on discolouration effect of electric light sources on oil painting and water colour painting in museum, *Light & Engineering*, 2024, 85-92, doi: 10.33383/2023-087.
[19] R. Kore, D. Durmus, Optimizing light source spectra for art conservation: exploring basic color groups, *Leukos*, 2025, **21**, 257-269, doi: 10.1080/15502724.2024.2366479.
[20] J. M. del Hoyo-Mel é ndez, Physico-chemical characterisation and light stability of dyes and pigments found in cultural heritage objects: Insights from microfading testing for assessing light fastness, *Coloration Technology*, 2025, **141**, 265-290, doi: 10.1111/cote.12788.
[21] M. T. Molina, E. Cano, J. Leal, R. Fort, M. Álvarez de Buergo, B. Ramírez-Barat, Protective coatings for metals in scientific: technical heritage: the collection of the Spanish national museum of science and technology (MUNCYT), *Heritage*, 2023, **6**, 2473-2488, doi: 10.3390/heritage6030130.
[22] O. Chiantore, L. Trossarelli, M. Lazzari, Photooxidative degradation of acrylic and methacrylic polymers, *Polymer*, 2000, **41**, 1657-1668, doi: 10.1016/s0032-3861(99)00349-3.
[23] L. Jiang, J. Feng, Z. B. Xiong, J. K. Wang, Y. Y. Wang, Research progress on aging resistance and service life evaluation of epoxy resin protective repair materials in hydraulic environment, *Materials Protection*, 2023, **56**, 142-153, doi: 10.16577/j.issn.1001-1560.2023.0225.
[24] X. Gong, X. N. Han, K. L. Chen, UV aging characterization of paraloid acrylic polymers for art conservation by infrared spectroscopy, *Spectroscopy and Spectral Analysis*, 2022, **42**, 2175, doi: 10.3964/j.issn.1000-0593(2022)07-2175-06.
[25] S. Zhuang, X. Lv, L. Pan, L. Lu, Z. Ge, J. Wang, J. Wang, J. Liu, W. Liu, C. Zhang, Benzotriazole UV 328 and UV-P showed distinct antiandrogenic activity upon human CYP3A4-mediated biotransformation, *Environmental Pollution*, 2017, **220**, 616-624, doi: 10.1016/j.envpol.2016.10.011.
[26] S. T. Butt, T. Christensen, Toxicity and phototoxicity of chemical Sun filters, *Radiation Protection Dosimetry*, 2000, **91**, 283-286, doi: 10.1093/oxfordjournals.rpd.a033219.
[27] A. Burgos-Cara, C. Rodríguez-Navarro, M. Ortega-Huertas, E. Ruiz-Agudo, Bioinspired alkoxysilane conservation treatments for building materials based on amorphous calcium carbonate and oxalate nanoparticles, *ACS Applied Nano Materials*, 2019, **2**, 4954-4967, doi: 10.1021/acsanm.9b00905.
[28] A. Speziale, J. F. González-Sánchez, B. Taşcı, A. Pastor, L. Sánchez, C. Fernández-Acevedo, T. Oroz-Mateo, C. Salazar, I. Navarro-Blasco, J. M. Fernández, J. I. Alvarez, Development of multifunctional coatings for protecting stones and lime mortars of the architectural heritage, *International Journal of Architectural Heritage*, 2020, **14**, 1008-1029, doi: 10.1080/15583058.2020.1728594.
[29] M. R. Ataabadi, M. Jamshidi, Improved photocatalytic degradation of methylene blue under visible light using acrylic nanocomposite contained silane grafted nano TiO_2, *Journal of Photochemistry and Photobiology A: Chemistry*, 2023, **443**, 114832, doi: 10.1016/j.jphotochem.2023.114832.

[30] Z. Li, X. Ma, Y. Geng, M. Huang, H. Liu, W. Liu, S. He, W. Xu, C. Zhu, Colorless and transparent self-healing polyurethane urea with superior tensile strength for protective coating, *European Polymer Journal*, 2025, **228**, 113827, doi: 10.1016/j.eurpolymj.2025.113827.
[31] D. Zhu, Z. Li, Y. Wang, W. Chen, N. Wu, M. Huang, H. Liu, S. He, W. Xu, W. Liu, Structural design of colorless transparent polyurethane with intrinsic UV resistance and high mechanical performance for protective coating, *Macromolecular Chemistry and Physics*, 2025, **226**, e00213, doi: 10.1002/macp.202500213.
[32] N. Nasirzadeh, M. R. Monazzam Esmaielpour, R. Faridi-Majidi, F. Golbabaei, Green synthesis of zinc oxide nanoparticles from sour cherry pomace extract as an effective light absorber and photocatalyst in textile industry, *Biomass Conversion and Biorefinery*, 2025, **15**, 17665-17678, doi: 10.1007/s13399-024-06406-3.
[33] X. D. Chen, Z. Wang, Z. F. Liao, Y. L. Mai, M. Q. Zhang, Roles of anatase and rutile TiO_2 nanoparticles in photooxidation of polyurethane, *Polymer Testing*, 2007, **26**, 202-208, doi: 10.1016/j.polymertesting.2006.10.002.
[34] D. Scalarone, M. Lazzari, O. Chiantore, Acrylic protective coatings modified with titanium dioxide nanoparticles: Comparative study of stability under irradiation, *Polymer Degradation and Stability*, 2012, **97**, 2136-2142, doi: 10.1016/j.polymdegradstab.2012.08.014.
[35] X. Lv, B. Yan, Y. Shao, H. Zhang, H. Zhang, J. Zhu, A core-shell composite pigment with rutile TiO_2 intensification for UV inhibition, *Particuology*, 2022, **67**, 18-26, doi: 10.1016/j.partic.2021.09.010.
[36] C. Zhang, Y. Wu, Y. Zhang, Y. Sun, Research status of nanometer silicon dioxide's modification of coatings, *Forestry Machinery & Woodworking Equipment*, 2013, **41**, 16-22.
[37] H. Zhang, X. Liu, Application and Prospect of Nano Technology in Architectural Coating, *Coating Industry*,2012, **42**, 72-74, 79, doi: 10.3969/j.issn.0253-4312.2012.05.019.
[38] H. J. Lee, J. W. Shim, J. J. Lee, W. J. Lee, The encapsulation of natural organic dyes on TiO_2 for photochromism control, *International Journal of Molecular Sciences*, 2023, **24**, 7860, doi: 10.3390/ijms24097860.
[39] S. Zhang, S. Hu, Y. Zhou, M. Xie, Y. Liao, F. Yue, Flavonoids-in-lignin coextraction strategy for developing long-lasting UVA-enhanced sunscreens, *ACS Sustainable Chemistry & Engineering*, 2025, **13**, 4560-4569, doi: 10.1021/acssuschemeng.4c10603.
[40] Y. Ma, C. Li, W. Su, Z. Sun, S. Gao, W. Xie, B. Zhang, L. Sui, Carotenoids in skin photoaging: unveiling protective effects, molecular insights, and safety and bioavailability frontiers, *Antioxidants*, 2025, **14**, 577, doi: 10.3390/antiox14050577.
[41] Z. Zhao, Y. Gao, M. Yuan, C. Ye, Y. Guo, Y. Zhao, J. Li, J. Cui, T. Dong, D. Wu, Application prospects of schisandra chinensis fruit post-distillation residues in anti-photoaging products: enhancing anti-photoaging through lignans conversion, *Waste and Biomass Valorization*, 2025, **16**, 2579-2592, doi: 10.1007/s12649-024-02846-0.
[42] Y. Luo, X.-C. Liu, Y.-J. Li, Y.-J. Wang, M.-H. Qiu, X.-R. Peng, Advances in natural products with anti-skin photoaging: mechanisms, phytochemical diversity, and therapeutic potential, *Phytochemistry Reviews*, 2025, doi: 10.1007/s11101-025-10170-1.
[43] M. J. Saadh, V. Jain, M. M. Rekha, P. K. Pathak, H. M. Ahmed, K. Satyam Naidu, B. Juneja, F. Faez Sead, M. Dehghanipour, Recent advancement on nanotechnology and natural compounds for skin UV protection: a review, *International Journal of Environmental Science and Technology*, 2025, **22**, 13223-13244, doi: 10.1007/s13762-025-06589-w.
[44] M. Lv, Y. Yang, P. Choisy, T. Xu, K. Pays, L. Zhang, J. Zhu, Q. Wang, S. Li, L. Wang, Flavonoid components and anti-photoaging activity of flower extracts from six Paeonia cultivars, *Industrial Crops and Products*, 2023, **200**, 116707, doi: 10.1016/j.indcrop.2023.116707.
[45] Y. Niu, J. Liao, H. Zhou, C.-C. Wang, L. Wang, Y. Fan, Flavonoids from lycium barbarum leaves exhibit anti-aging effects through the redox-modulation, *Molecules*, 2022, **27**, 4952, doi: 10.3390/molecules27154952.
[46] X.-Y. Zhang, D.-S. Wang, X. Li, Y.-C. Miao, J.-M. Gao, Q. Zhang, A new utilization of total flavonoids from Acer truncatum samara and leaves: Anti-aging and metabolic regulation, *Industrial Crops and Products*, 2023, **203**, 117207, doi: 10.1016/j.indcrop.2023.117207.
[47] S. Lakshman, Y. L. N. Murthy, K. Ram Mohan Rao, Studies on synthesis and antioxidant property of anthraquinone analogues, *Materials Today: Proceedings*, 2021, **40**, S75-S78, doi: 10.1016/j.matpr.2020.03.719.
[48] Q. Jia, P.-Y. Yang, X. Zhang, S.-J. Song, X.-X. Huang, Aromatic glycosides and lignans glycosides with their acetylcholinesterase inhibitory activities from the leaves of Picrasma quassioides, *Fitoterapia*, 2024, **172**, 105701, doi: 10.1016/j.fitote.2023.105701.
[49] F. Zhang, T. Ren, P. Gao, N. Li, Z. Wu, J. Xia, X. Jia, L. Yuan, P. Jiang, Characterization and anti-aging effects of polysaccharide from Gomphus clavatus Gray, *International Journal of Biological Macromolecules*, 2023, **246**, 125706, doi: 10.1016/j.ijbiomac.2023.125706.
[50] C. Zhang, X. Song, W. Cui, Q. Yang, Antioxidant and anti-ageing effects of enzymatic polysaccharide from Pleurotus eryngii residue, *International Journal of Biological Macromolecules*, 2021, **173**, 341-350, doi: 10.1016/j.ijbiomac.2021.01.030.
[51] C. Jin, R. G. Michetich, M. Daneshtalab, Flavonoids from stellera chamaejasme, *Phytochemistry*, 1999, **50**, 505-508, doi: 10.1016/s0031-9422(98)00588-3.
[52] H. Guo, H. Cui, H. Jin, Z. Yan, L. Ding, B. Qin, Potential allelochemicals in root zone soils of *Stellera chamaejasme L*. and variations at different geographical growing sites, *Plant Growth Regulation*, 2015, **77**, 335-342, doi: 10.1007/s10725-015-0068-4.
[53] Q. Song, S.-F. Li, Z.-Y. Cheng, S.-J. Song, X.-X. Huang, Chemical constituents from *Stellera chamaejasme L.* and chemotaxonomic significance, *Biochemical Systematics and Ecology*, 2023, **107**, 104602, doi: 10.1016/j.bse.2023.104602.

[54] T. Selenge, S. F. Vieira, O. Gendaram, R. L. Reis, S. Tsolmon, E. Tsendeekhuu, H. Ferreira, N. M. Neves, Antioxidant and anti-inflammatory activities of *Stellera chamaejasme L*. roots and aerial parts extracts, *Life*, 2023, **13**, 1654, doi: 10.3390/life13081654.
[55] J. Wu, Z. Ye, C. Liao, R. Li, X. Chen, Terpenoids from the roots of stellera chamaejasme (L.) and their bioactivities, *Molecules*, 2023, **28**, 7726, doi: 10.3390/molecules28237726.
[56] Y.-H. Zhang, S.-D. Zhang, L.-Z. Ling, *De novo* transcriptome analysis to identify flavonoid biosynthesis genes in Stellera chamaejasme, *Plant Gene*, 2015, **4**, 64-68, doi: 10.1016/j.plgene.2015.09.006.
[57] K. Shirai, Y. Okamoto, M. Tori, T. Kawahara, X. Gong, T. Noyama, E. Watanabe, C. Kuroda, Diversity in the flavonoid composition of *Stellera chamaejasme* in the Hengduan Mountains, *Natural Product Communications*, 2015, **10**, 1934578X1501000115, doi: 10.1177/1934578x1501000115.
[58] National Technical Committee on Coatings and Pigments of Standardization Administration of China, Methods for measuring the color of paint films—Part 2: Colour measurement: GB/T 11186.2-1989, Standards Press of China, 1989.
[59] National Technical Committee on Coatings and Pigments of Standardization Administration of China. Methods for measuring the color of paint films—Part 3: Calculation of color differences: GB/T 11186.3-1989, Standards Press of China, 1989.
[60] National Technical Committee on Coatings and Pigments of Standardization Administration of China. Paints and varnishes—Rating schemes of degradation of coats: GB/T 1766-2008, Standards Press of China, 2008.

Publisher's Note: Engineered Science Publisher remains neutral with regard to jurisdictional claims in published maps and institutional affiliations.

Open Access
This article is licensed under a Creative Commons Attribution-NonCommercial-NoDerivatives 4.0 International, which permits the use, sharing, adaptation, distribution and reproduction in any medium or format, as long as appropriate credit to the original author(s) and the source is given by providing a link to the Creative Commons license. This usage for commercial purposes is not allowed. If modifications, adaptations or any other transformation were made, it is not allowed for distribution. The images or other third-party material in this article are included in the article's Creative Commons license, unless indicated otherwise in a credit line to the material. If material is not included in the article's Creative Commons license and your intended use is not permitted by statutory regulation or exceeds the permitted use, you will need to obtain permission directly from the copyright holder. To view a copy of this license, visit https://creativecommons.org/licenses/by-nc-nd/4.0/.

©The Author(s) 2025.